Mon. Not. R. Astron. Soc. **000**, 000–000 (0000) Printed 23 February 2012 (MN LaTeX style file v2.2)

arXiv:1202.4770v1 [astro-ph.CO] 21 Feb 2012

The physics of the fundamental metallicity relation

Pratika Dayal[1⋆], Andrea Ferrara[2], James S Dunlop[1]
[1] *SUPA†, Institute for Astronomy, University of Edinburgh, Royal Observatory, Edinburgh, EH9 3HJ, UK*
[2] *Scuola Normale Superiore, Piazza dei Cavalieri 7, 56126 Pisa, Italy*

ABSTRACT
We present a simple, redshift-independent analytic model that explains the local Fundamental Metallicity Relation (FMR), taking into account the physical processes of star formation, inflow of metal-poor intergalactic medium (IGM) gas, and the outflow of metal rich interstellar medium (ISM) gas. We show that the physics of the FMR can be summarised as follows: for massive galaxies with stellar mass $M_* \geqslant 10^{11}\mathrm{M}_\odot$, ISM metal enrichment due to star formation is compensated by inflow of metal poor IGM gas, leading to a constant value of the gas metallicity with star formation rate (SFR); outflows are rendered negligible as a result of the large potential wells of these galaxies. On the other hand, as a result of their smaller SFR, less massive galaxies produce less heavy elements that are also more efficiently ejected due to their shallow potential wells; as a result, for a given M_*, the gas metallicity decreases with SFR. For such galaxies, the outflow efficiency determines both the slope, and the knee of the metallicity-SFR relation. The model is then successfully matched to results from numerical simulations including metal enrichment and feedback at higher redshifts.

Key words: galaxies:high-redshift - fundamental parameters - evolution - abundances - stellar content

1 INTRODUCTION

Observationally, the stellar mass and the gas phase metallicity are two of the most fundamental properties of galaxies, reflecting the amount of baryons locked up in stars, and the amount of metals present in the interstellar medium (ISM) gas, respectively. They also provide insights into a number of parameters pertinent for understanding galaxy evolution including the stellar initial mass function (IMF) which determines the amount of metals produced and returned by stars to the ISM, the star formation history which determines the total stellar mass and metal content, and the amount of metal rich gas ejected/mass of metal poor gas accreted. The existence of a mass-metallicity relation has now been observationally established by many authors including Garnett (2002), Tremonti et al. (2004), Cowie & Barger (2008) and Pérez-Montero et al. (2009). The origin of this relation, however, has been widely debated and a number of different explanations have been proposed for its existence, including: the ejection of metal rich gas (e.g. Garnett 2002; Spitoni et al. 2010), a dependence of the star formation rate (SFR) on the galaxy mass (e.g. Calura et al. 2009), infall of metal poor intergalactic medium (IGM) gas into the galaxy (e.g. Dekel et al. 2009; Mannucci et al. 2009), and a balance between ISM metal enrichment due to star formation and dilution due to infall of metal poor IGM gas (Finlator & Davé 2008).

Recently, using observations of galaxies at $0 < z < 4$, Mannucci et al. (2010) have shown that the mass-metallicity relation arises as a consequence of a more fundamental 3D relation, referred to as the fundamental metallicity relation (FMR), relating the stellar mass, gas-phase metallicity and the SFR; indeed, if infall is the main driver for star formation, and it is star formation that drives outflows, such a relation is only to be expected.

In this work, our aim is to build a simple and yet physically consistent analytic model that explains the observed FMR, taking into account the relevant physical processes of gas inflow/outflow, star formation and metal production. The main advantage of the model presented here lies in the fact that its results are essentially independent of the redshift considered for $z \leqslant 6$, for reasons that are explained in what follows. We also show that the results from this analytic model are in excellent agreement with those obtained from state-of-the-art cosmological simulations.

2 BASIC PHYSICAL INTERPRETATION

As explained above, our first aim is to build the *simplest* model that can account for the observed FMR trends. The observable quantities determining the FMR of a given galaxy, i.e. stellar mass (M_*), SFR (ψ), and oxygen abun-

---

⋆ E-mail:prd@roe.ac.uk (PD)
† Scottish Universities Physics Alliance

dance (often used as a proxy for metallicity), $X = M_O/M_g$, where M_O and M_g are the galaxy oxygen and gas mass, respectively, are related by a simple set of evolutionary ordinary differential equations:

$$\frac{dM_*}{dt} \equiv \psi = \epsilon_* M_g \tag{1}$$

$$\frac{dM_g}{dt} = -(1-R)\psi + (a-w)\psi \tag{2}$$

$$M_g \frac{dX}{dt} = y(1-R)\psi - aX\psi, \tag{3}$$

where ϵ_*^{-1} is the star formation timescale and the SFR is assumed to be proportional to the gas mass. The two constants, R and y, represent the returned fraction from stars and the the yield per stellar generation, respectively, and are dependent on the IMF; whenever numerical values are required, we use $(R, y) = (0.79, 0.0871)$ consistent with a Salpeter IMF for a lower (upper) mass limit of 1 (100) $\mathrm{M}_\odot$. We assume that both the outflow, $w(M)\psi$, and infall, $a(M)\psi$, rates are proportional to the SFR, where M is the total (dark+baryonic) galaxy mass; while the former assumption is easy to understand, the latter has been made to obtain the simplest solution to the equations described above. We further pose that the metallicity of the infalling gas is $X_i \ll X$. Simple algebraic manipulation of the above equations gives the general solution

$$X(\psi) = \frac{y(1-R)}{a}\left(1 - \mu^{-\alpha}\right), \tag{4}$$

where $\mu = M_g/M_{g0} = \psi[\epsilon_* M_{g0}]^{-1}$. The initial gas mass can be expressed as $M_{g0} \simeq M_*(1+w-a) + M_g = (\Omega_b/\Omega_M)M$, and $\alpha = a[R-1+a-w]^{-1}$. We now interpret the physical meaning of the above relation.

Firstly, we note that reproducing the observed decreasing trend of $X(\psi)$ for the smallest galaxies requires $\alpha < 0$, i.e. the condition $a < w + (1-R)$ has to be satisfied. Note that this condition also ensures that $\mu^{-\alpha} \leqslant 1$ at any time. In addition, if $\mu \ll 1$, as is the case for large galaxies in which most of the gas has been turned into stars, $X(\psi) \approx y(1-R)a^{-1} =$ constant, as indeed observed. This property can then be used to normalize the value of a for the largest galaxies to the observed oxygen abundance, X^{obs} by requiring $a = y(1-R)/X^{obs}$. Physically, the larger the value of a, smaller is the value of X, i.e. the metallicity of the galaxy is diluted by low metallicity infalling gas. We note that the no-infall case ($a = 0$) would not admit solutions in which metallicity is independent of the SFR; such constancy implies that some infall is required.

Outflows affect the solution through the term $\mu^{-\alpha}$ in two ways: (a) by setting the position, ψ^*, of the knee in the $X(\psi)$ curve, above which the metallicity starts to drop at a fixed M_*; this is determined by the condition $\mu = 0.5$, or $\psi^* = \epsilon_*(1+w-a)M_*$. Thus, for large outflow efficiencies (w), the knee shifts to lower values of ψ; at fixed w, less massive galaxies deviate from a constant $X(\psi)$ relation at lower ψ values. (b) The outflow efficiency w also regulates the slope of the curve through the power α: as w is increased the slope becomes steeper. The combined effect is that, for a given value of ψ, low-mass galaxies are more metal poor than massive ones.

By fitting the $X(\psi)$ curves for various M_* to the Mannucci et al. (2010) data, we can also tune the dependence of the only two free parameters of the model: $a(M)$ and $w(M)$. In a previous paper (see Fig. 6, Dayal et al. 2009), using the same numerical simulation, we have shown that $M_* \propto M$; as a result, we can assume that the two quantities track each other. We find that the best fit to the data require

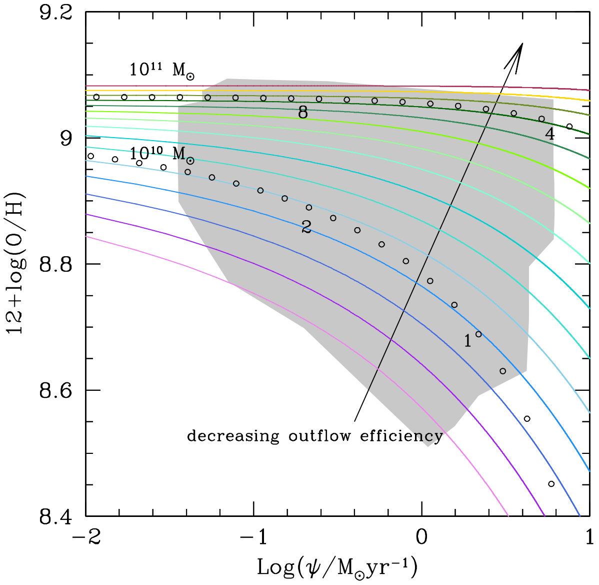

Figure 1. Oxygen abundance versus SFR for galaxies of different stellar masses, in the range $M_* = 10^{9.25+0.15j}\mathrm{M}_\odot$, with $j = 0, .., 14$, from the bottom to the top curves; the shaded region shows the oxygen abundance-SFR relation inferred observationally by Mannucci et al. (2010) for local SDSS galaxies for the same stellar mass range, i.e $10^{9.25-11.35}\mathrm{M}_\odot$. Points show the evolutionary tracks of two representative galaxies with initial gas masses of $10^{10,11}\mathrm{M}_\odot$ respectively, and numbers along the track indicate the values of $\tau = \epsilon_* t$ at selected ages.

$$\ln a = -0.43 - 0.05\ln(M_*/10^{10.75})\mathrm{M}_\odot, \tag{5}$$

$$\ln w = 1.76 - 0.33\ln(M_*/10^{9.0})\mathrm{M}_\odot, \tag{6}$$

Hence, the accretion efficiency is essentially independent of the galaxy mass, implying that the accretion rate scales almost linearly with M. The ejection efficiency is small in large galaxies ($w \approx 1.0$ for $M_* = 10^{11.35}\mathrm{M}_\odot$) and rapidly increases with decreasing M_*, reaching $w = 4.8$ for the smallest ones ($M_* = 10^{9.25}\mathrm{M}_\odot$). It is interesting to note that the mass dependence we find, $w \propto M_*^{-1/3} \propto v_e^{-1}$, is the one expected if the outflow is momentum-driven.

The metallicity-SFR relation (solid curves) as a function of the galaxy stellar mass is shown in Fig. 1, along with the evolutionary tracks (points) of two representative galaxies whose initial gas mass is $M_{g0} = 10^{10,11}\mathrm{M}_\odot$ (time runs from right to left along the open circles). Galaxies start from low O/H, low stellar mass, and high SFR values and then move towards higher metallicities as their stellar mass increases. However, depending on their mass they move at different velocities along the track: the most massive observed galaxies are very evolved with a specific age (i.e. in units of the star formation timescale $\epsilon_*^{-1} = 0.62$ Gyr) $\tau = \epsilon_* t \gtrsim 4$, and move essentially along constant metallicity curves; smaller objects are younger ($1 < \tau < 2$) and are still gently building up their metal content.

2.1 Remarks

The simple model presented above reproduces the locally observed FMR extremely well, essentially through the single, redshift-independent Eq. 4. Time (or z) only specifies when in the course of its evolution a galaxy reaches a given (X, ψ) point in the plane. As we see later, the same $X - \psi$ trend emerges from numerical simulations at high-z, thus supporting the idea that the FRM is indeed a fundamental property of galaxies due to the local interplay of star formation, infall and outflows.

Although these conclusions are similar to those reached by Davé et al. (2011, D11), there are important conceptual differences. Firstly, D11 make the *Ansatz* that the galaxy system is always in a stationary state, i.e. the infall rate exactly balances the gas lost in outflows and star formation; this is equivalent to setting $dM_g/dt = 0$ in Eq. 2 above, or $a = (1 - R) + w$. Analogously, $dX/dt = 0$ is imposed on the metallicity (Eq. 3), yielding $X = y(1 - R)a^{-1}$ in D11. By inspecting Eq. 4, we see that this expression approximates the relation for large galaxies with $\mu \ll 1$, but fails to catch the metallicity decrease with increasing SFR seen in smaller, outflow-dominated galaxies. A posteriori, the values for the infall and outflow rate we find by fitting the $z = 0$ FMR data are such that $a < (1 - R) + w$, due to the large outflow rates deduced. Moreover, D11 impose a given external infall rate derived from numerical simulations (devised to model relatively large galaxies), while we do not make any assumption on its mass and redshift dependence; in both models though, the infall rate is proportional to ψ. It is not clear at this stage how the D11 model would perform when compared to the FRM data reproduced here, but it would be useful to compare the two approaches in detail. As a final point, we stress that our set of time-dependent ODEs (2)-(3) require an initial condition $M_{g0} \neq 0$ in order to lead to physically meaningful solutions. This implies that our SFR always exponentially decrease in time, starting from a finite value. There could instead be a relatively short (< 1 Gyr) transient period corresponding to the build-up phase with increasing SFR (D11), which is not captured by our simple assumptions. Thus a more complex version of the model (or numerical simulations, see below) should be used if one is interested in the FMR at $z \gtrsim 6$.

3 SIMULATING THE FMR

As argued above, the analytic model presented in Sec. 2 is expected to work well for galaxies that have already assembled their gas mass, once the transient gas build-up phase lasting about a Gyr is complete. We now check the validity of such a statement using a state-of-the-art cosmological simulation with a periodic box size of $75h^{-1}$ comoving Mpc. This is now briefly described and interested readers are referred to Tornatore et al. (2010) for a complete description: the simulation has been carried out using the TreePM-SPH code GADGET-2 (Springel 2005) with the implementation of chemodynamics as described in Tornatore et al. (2007). The adopted cosmological model corresponds to a ΛCDM Universe, consistent with the 5-year analysis of the WMAP data (Komatsu et al. 2009). The run includes metallicity-dependent radiative cooling (Sutherland & Dopita 1993), has an effective model to describe star formation from a multi-phase ISM and a prescription for galactic winds triggered by supernova (SN) explosions (Springel & Hernquist 2003). The IMF is taken to be Salpeter in the range $1 - 100\,\mathrm{M}_\odot$. Metals and energy are released by stars of different masses by properly accounting for mass-dependent lifetimes as proposed by Padovani & Matteucci (1993). The code uses the metallicity-dependent yields from Woosley & Weaver (1995); the yields for SNIa and asymptotic giant branch stars have been taken from van den Hoek & Groenewegen (1997). For each galaxy, identified as a gravitationally bound group of particles (see Saro et al. 2006), in each of the snapshots of interest, we obtain the total halo/gas/stellar mass ($M_h/M_g/M_*$), the SFR (ψ) and the mass weighted gas/stellar metallicity (Z_g/Z_*); $z \approx 4.5$ is the lowest redshift snapshot available due to simulation constraints. When compared to the standard Sheth-Tormen mass function (Sheth & Tormen 1999), the simulated mass function is complete for halo masses $M_h \geqslant 10^{10}\mathrm{M}_\odot$ in the entire redshift range of interest; galaxies above this mass cut-off are then referred to as the "complete sample" and used for all the calculations presented in this paper.

Comparing the FMR inferred from the numerical simulation at $z \approx 4.5$ to the analytic one presented in Sec. 2, we find that these are in excellent agreement for $M_* \approx 10^{8.5-10.45}\mathrm{M}_\odot$, as shown in Panel (a) of Fig. 2; the analytic results for three specific mass bins, $M_* = 10^{8.45,9.25,10.3}\mathrm{M}_\odot$ have been plotted in the same panel to guide the eye. Such agreement lends support to a scenario wherein galaxies evolve from a short-lasting transient gas-accretion phase to one in which an interplay between SFR, inflows and outflows are the dominant physical processes shaping the FMR: as explained in Sec. 2, outflows affect the metallicity-SFR relation such that for a given value of M_*, galaxies with the largest SFR are the most metal poor and the metallicity-SFR relation flattens with increasing M_* due to a decrease in the outflow efficiency; however, the flattening of the FMR is not possible without at least some inflow of metal-poor gas.

The same FMR trends hold also at $z \approx 5.7, 6.6$ as seen from panels (b,c) of Fig. 2, albeit that as expected in a hierarchical structure formation scenario where large galaxies build up from the merger of smaller systems, the stellar mass range narrows with increasing redshift, from $M_* \approx 10^{8.5-10.6}\mathrm{M}_\odot$ at $z \approx 4.5$ to $M_* \approx 10^{8.5-9.7}\mathrm{M}_\odot$ at $z \approx 6.6$; as a consequence of the narrower M_* (and SFR) range, the gas metallicity range also decreases to $\approx 0.05 - 0.6(0.06 - 0.4)\mathrm{Z}_\odot$ at $z \approx 4.5(6.6)$. Finally, although our simulations reproduce the observed metallicity-SFR trend extremely well at all the redshifts considered, we do not see a flattening of such relation, as seen in the $z = 0$ sample (Fig. 1). This is readily explicable considering that the flattening occurs for $M_* \geqslant 10^{11}\mathrm{M}_\odot$, independent of redshift (see also Sec. 2); such galaxies have not yet assembled by the lowest redshift presented here, $z \approx 4.5$, in the volume sampled by the simulation.

As expected from the discussion in Sec. 2, for a given SFR, galaxies with larger M_* have a larger gas metallicity by virtue of their larger potential wells that prevent metal loss due to outflows; this trend holds for all redshifts, $z \approx 4.5 - 6.6$. Again, the SFR range reduces with increasing redshift, as a consequence of the narrowing of the stellar mass range such that $\psi \approx 0.6 - 200\mathrm{M}_\odot\mathrm{yr}^{-1}$ at $z \approx 4.5$ and

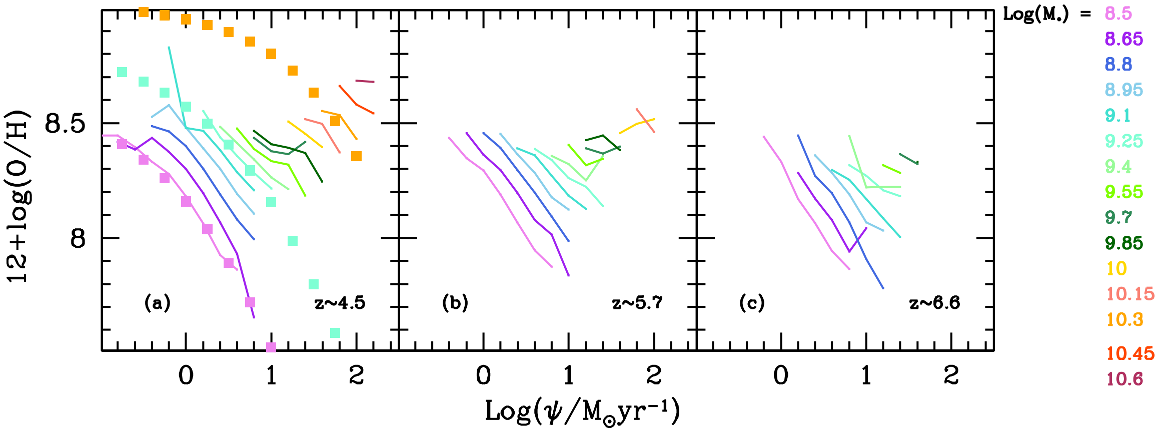

Figure 2. As a function of the SFR (ψ), we show the gas metallicity, $12 + \log(\mathrm{O/H})$, in different stellar mass bins (M_*), as obtained from numerical simulations. Panels from left to right show the simulated results for $z \approx 4.5 - 6.6$, as marked. Filled squares in the left-most panel show the SFR-gas metallicity relation obtained using the analytic model presented in Sec. 2 for three stellar mass bins, $\mathrm{Log}(M_*) = 8.5, 9.25, 10.3\,\mathrm{M}_\odot$ from bottom to top respectively. This shows the simulated and analytic results are in excellent agreement at $z \approx 4.5$. See text for details.

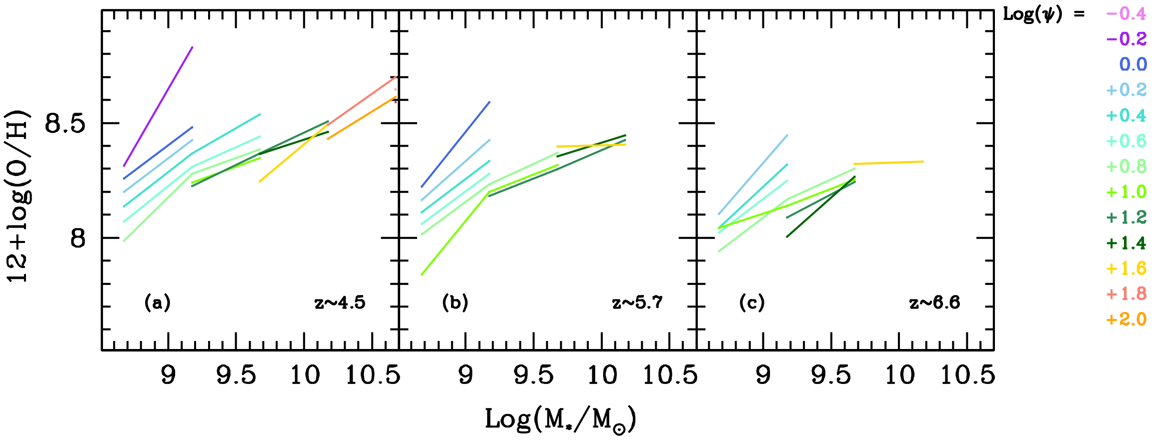

Figure 3. As a function of the stellar mass (M_*), we show the gas metallicity in units of $12 + \log(\mathrm{O/H})$, in different SFR (ψ) bins, as obtained from numerical simulations. Panels from left to right show the simulated results for $z \approx 4.5 - 6.6$, as marked.

reduces to $\psi \approx 1.6 - 40\mathrm{M}_\odot\mathrm{yr}^{-1}$ at $z \approx 6.6$. Finally, due to a lack of galaxies with $M_* \geqslant 10^{11}\mathrm{M}_\odot$, again, we do not see a clear flattening of the metallicity-stellar mass relation, as observed for such galaxies at $z = 0$ by Mannucci et al. (2010).

Finally, we show the gas metallicity as a function of the parameter $\zeta = \log(M_*) - 0.32\log(\psi)$ that Mannucci et al. (2010) have introduced to minimize the metallicity scatter. We find that the simulated galaxies follow a tight metallicity-ζ relation for all the redshifts considered, as shown in Fig. 4. When compared to the relation inferred using local SDSS galaxies, $z \approx 4.5 - 6.6$ galaxies essentially follow the same slope on the metallicity-ζ plane, although as expected, both the metallicity and ζ ranges decrease with increasing redshift; the metallicity scatter between $z \approx 4.5 - 6.6$ is about 0.35 dex at most (at $\zeta \approx 9.0$). Further, at $\zeta \approx 9.7$, the simulated metallicity at $z \approx 4.5$ falls short by about 0.3 dex of that measured by Mannucci et al. (2010) for local SDSS galaxies. This is in slight tension with Mannucci et al. (2010), who find a metallicity difference of about 0.6 dex at $\zeta \approx 9.7$ between $z \approx 3$ and local galaxies, although they find no evolution in the metallicity with ζ, for $z = 0 - 2.5$. Possible reasons for such a discrepancy are discussed briefly below in Sec. 4.

4 CONCLUSIONS

We have presented a very simple model that provides a straightforward explanation of the 3D FMR relating the stellar mass, SFR and gas metallicity observed by Mannucci et al. (2010) in the local Universe. Starting from a galaxy that has already assembled its gas mass after a transient gas-accretion phase, assuming the metallicity of the infalling IGM gas to be much lower than that of the ISM gas, and assuming both the inflow and outflow rates to be proportional to the SFR, we calibrate the only two model free parameters (the inflow and outflow rates) to the local FMR data. Using this model, we show that both inflows and outflows are required to explain the observations, although their importance is mass dependent: since we as-

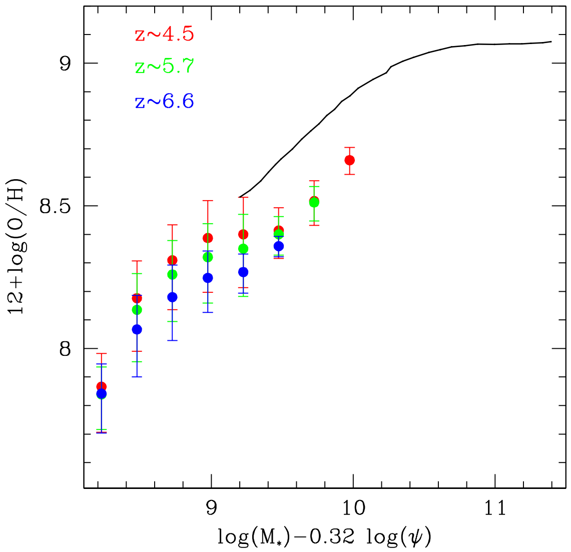

Figure 4. As a function of the parameter $\zeta = \log(M_*) - 0.32\log(\psi)$, we show the gas metallicity, 12 + log(O/H), for $z \approx 4.5-6.6$, as obtained from numerical simulations; the solid line shows the measurements of Mannucci et al. (2010) for local SDSS galaxies.

sume the inflow rate to be proportional to the SFR (and hence M_*), galaxies with the largest M_* accrete the largest amount of metal-poor IGM gas, which is balanced by the larger amount of metals produced due to star formation; this, coupled with the negligible outflow rates due to their large potential wells, makes the metallicity-SFR relation essentially constant for galaxies with $M_* \geqslant 10^{11}\mathrm{M}_\odot$. On the other hand, due to their smaller SFR, less massive galaxies produce less metals. However, as a result of their smaller potential wells, outflows lead to a loss of metal-rich ISM gas so that at a given M_*, galaxies with the largest SFR are the most metal poor; alternatively, for a given SFR, smaller galaxies are more metal poor than massive ones.

Since the analytic model developed is valid for all galaxies that have 'assembled' their gas mass after a transient phase of gas-accretion, we can compare its results with those from state-of-the-art cosmological simulations; due to computational constraints, such comparison is only possible down to $z \approx 4.5$. However, even at this high-redshift, the analytic results are in excellent agreement with those from the simulation, providing a validation for our analytic model. The same FMR trends hold up to $z \approx 6.6$, although as expected, galaxies become smaller and have lower gas metallicities with increasing redshift.

We conclude by discussing the main caveats: firstly, as already mentioned, we ignore the complication of including the initial phase of gas accretion that is important for relatively large galaxies. However, as is shown by the excellent agreement between the analytic model and results from numerical simulations, such considerations are important at high-redshifts ($z \geqslant 5$) when galaxies are still building up their final mass. Secondly, to find an analytic solution to Eqs. 2-4, we have used an infall rate that is proportional to the SFR, although we do not make any assumption on its galaxy mass and redshift dependence. In the future, we aim at exploring models wherein such an assumption is not made. Finally, at $\zeta = 9.7$, we find a smaller metallicity difference (about 0.3 dex) between the $z \approx 4.5$ simulated results and $z = 0$ observations, compared to the value of 0.6 dex found by Mannucci et al. (2010) between the data at $z = 0$ and 3. Although such a difference could arise from observational biases at $z \approx 3$, i.e. small number statistics (16 observed galaxies), or the use of the OIII line that is biased towards lower metallicity galaxies (see Sec. 5.1 Mannucci et al. 2010), it could also be in part attributed to the difference in the simulated and observed mass ranges, and the effects of the resolution and feedback implementation in numerical simulations, on the SFR and gas metallicity. However, a much larger observed data set is required before any such meaningful comparison can be made.

ACKNOWLEDGMENTS

We thank our collaborators S. Borgani, L. Tornatore, A. Saro, and C. Evoli, R. Schneider, G. Cresci and F. Mannucci for useful discussions. JSD and PD acknowledge the support of the European Research Council via the award of an Advanced Grant, and JSD also acknowledges the support of the Royal Society via a Wolfson Research Merit award. PD thanks the SNS Pisa for hospitality.

REFERENCES

Calura F., Pipino A., Chiappini C., Matteucci F., Maiolino R., 2009, A&A, 504, 373
Cowie L. L., Barger A. J., 2008, ApJ, 686, 72
Davé R., Finlator K., Oppenheimer B. D., 2011, MNRAS, 2110
Dayal P., Ferrara A., Saro A., Salvaterra R., Borgani S., Tornatore L., 2009, MNRAS, 400, 2000
Dekel A., Sari R., Ceverino D., 2009, ApJ, 703, 785
Finlator K., Davé R., 2008, MNRAS, 385, 2181
Garnett D. R., 2002, ApJ, 581, 1019
Komatsu E. et al., 2009, ApJS, 180, 330
Mannucci F., Cresci G., Maiolino R., Marconi A., Gnerucci A., 2010, MNRAS, 408, 2115
Mannucci F. et al., 2009, MNRAS, 398, 1915
Padovani P., Matteucci F., 1993, ApJ, 416, 26
Pérez-Montero E. et al., 2009, A&A, 495, 73
Saro A., Borgani S., Tornatore L., Dolag K., Murante G., Biviano A., Calura F., Charlot S., 2006, MNRAS, 373, 397
Sheth R. K., Tormen G., 1999, MNRAS, 308, 119
Spitoni E., Calura F., Matteucci F., Recchi S., 2010, A&A, 514, A73
Springel V., 2005, MNRAS, 364, 1105
Springel V., Hernquist L., 2003, MNRAS, 339, 312
Sutherland R. S., Dopita M. A., 1993, ApJS, 88, 253
Tornatore L., Borgani S., Dolag K., Matteucci F., 2007, MNRAS, 382, 1050
Tornatore L., Borgani S., Viel M., Springel V., 2010, MNRAS, 402, 1911
Tremonti C. A. et al., 2004, ApJ, 613, 898
van den Hoek L. B., Groenewegen M. A. T., 1997, A&AS, 123, 305
Woosley S. E., Weaver T. A., 1995, ApJS, 101, 181